ELSEVIER

Tectonophysics 329 (2000) 171–191

TECTONOPHYSICS

www.elsevier.com/locate/tecto

Structure of the Makran subduction zone from wide-angle and reflection seismic data

C. Kopp[a,*], J. Fruehn[b,1], E.R. Flueh[a], C. Reichert[c], N. Kukowski[a,2], J. Bialas[a], D. Klaeschen[a]

[a]*GEOMAR — Research Center for Marine Geosciences, Kiel, Germany*
[b]*Bullard Laboratories, University of Cambridge, Cambridge, UK*
[c]*Federal Institute for Geosciences and Natural Resources-BGR, Hannover, Germany*

Received 13 February 1999; accepted 17 November 1999

Abstract

Makran is one of the largest accretionary wedges on the globe, formed by the convergence between the Eurasian and the Arabian Plates. It is characterised by an extremely high sediment input of 7 km and a shallow subduction angle. We present seismic velocity models from four wide-angle seismic lines that image the wedge sediments and the subducted oceanic crust. Three strike-lines show complex but rather one-dimensional structures, where the observed seismic phases have been studied with the reflectivity method. A 160 km long dip line was surveyed coincident with a MCS line collected by Cambridge University in 1986. Prestack depth migration of this data with the new wide-angle velocities shows improved images compared to earlier results.

Interpretation of the wide-angle and the MCS data indicates that a décollement is developed along a bright reflector within the turbiditic sequence. More than 3 km of sediment bypasses the first accretionary ridges (underthrusting) and is transported to greater depth. This might help to explain the sparse earthquake activity associated with subduction here. In the strike lines, low-velocity layers occur landward of the deformation front, in zones where active thrusting or underplating takes place. The oceanic crust is characterised by a strong velocity contrast between layer II and layer III.

Keywords: convergent margins; Makran; refraction seismics; underplating

1. Introduction

Together with the on-shore Makran Ranges, the Makran accretionary wedge forms one of the most extensive accretionary complexes on earth. Seismologists were puzzled by its sparse seismicity relative to the neighbouring regions, which are regularly devastated by large earthquakes (Jacob and Quittmeyer, 1979). Geophysicists discovered a crust of uniform magnetisation beneath the Gulf of Oman (Hutchinson et al., 1981), and a thick sedimentary column entering the subduction zone (Closs et al., 1969; White and Louden, 1983). Multiple efforts to image the accretionary structures have been made to understand the

* Corresponding author. Tel.: +49-431-600-2327; fax: +49-431-600-2928.
E-mail address: ckopp@geomar.de (C. Kopp).
[1] Presently at GX Technology, London, UK.
[2] Presently at GeoForschungsZentrum Potsdam, Germany.

0040-1951/00/$ - see front matter
PII: S0040-1951(00)00195-5

processes of accretion/subduction under the condition of extreme sediment input (White and Louden, 1983; Platt et al., 1985; Minshull et al., 1992; Fruehn et al., 1997). Exploration scientists have studied the hydrocarbon potential of the Makran shelf and slope in detail, mapping possible reservoir structures, but they had to abandon drilling because of overpressured young sediments (Harms et al., 1984).

In September 1997 a scientific cruise (SONNE-123) conducted by GEOMAR (Kiel, Germany), the German Federal Institute for Geosciences and Natural Resources (BGR, Hannover, Germany), the University of Cambridge (Cambridge, UK) and the National Institute of Oceanography (NIO, Karachi, Pakistan), set out for a survey that included swath mapping, high-resolution and single-channel reflection seismics, ocean-bottom seismology, micro-seismicity monitoring, magnetics and gravity. The work is part of the MAMUT (Makran–Murray–Traverse) project which has the objective of studying the evolution and recent processes of Murray Ridge and the Makran accretionary wedge (Flueh et al., 1997; Roeser, 1997; von Rad and Doose, 1998). In this paper, we present results from an ocean-bottom seismologic study of the Makran wedge. The aim is to present the seismic velocity structure of the subduction zone derived from ray tracing and inversion of the OBH data and to discuss the different implications of our findings for the structure of the accretionary system. Integration of these results with a coincident multi-channel seismic reflection profile (CAM30, Minshull et al., 1992) allows us to identify the plate boundary between the Arabian and Eurasian plates (i.e. the basal décollement) and to distinguish between the accreted and subducted volumes of incoming sediment.

In our interpretation of accretionary structures we use the terminology of von Huene and Scholl (1993). The sediment wedge forms by accretion (frontal accretion and underplating) against a backstop that is the seaward edge of the convergent margin's older rock framework (core buttress). Frontally accreted sediment is attached to the margin at the deformation front, whereas underplated sediment is added to its base. Underthrusting refers to sediment moving landward beneath a detachment (basal décollement) that can be either underplated or ultimately subducted (transported landward beneath the backstop together with the subducting plate).

2. Tectonic setting and evolution

The Makran accretionary complex (Fig. 1) has developed throughout the Cenozoic at the convergent margin between the Arabian and the Eurasian Plates. Its evolution has been coeval with the Himalayan orogeny (Harms et al., 1984). Its first evolutionary phase (late Oligocene to middle Miocene) was characterised by turbiditic deposition of quartzolithic sands and muds. It is believed that these sediments accumulated in a submarine fan (the Proto Indus Fan — Harms et al., 1984), on top of oceanic crust which probably formed at the Proto Carlsberg Ridge. Analysis of detrital modes of Tertiary sandstones and modern sands across the Himalayan belt suggests that the turbidites travelled south–west along the Himalayan Main Central Fault and were deposited in the present-day Gulf of Oman (Garzanti et al., 1996). Between the late Miocene and the middle Pleistocene these sediments were entrained by frontal accretion and underplating (Platt et al., 1985), and were covered by huge volumes of shelf-and-slope sand. The accretionary wedge grew seaward by accretion of trench fill sediments, and by slope, shelf and coastal plain progradation.

Since the middle Pleistocene the coastal Makran has experienced uplift and normal faulting, while in the seaward part accretion has continued to this day (Harms et al., 1984). At present, the accretionary complex has an along-strike extent of about 1000 km and is separated by two fault systems from regions of active continent–continent collision (the Zagros and Himalaya). The Minab Fault system bounds the Makran in the west, and the transpressional strike-slip system of the Ornach-Nal and Chaman Faults bounds it in the east (Fig. 1). Towards the south the latter boundary is continued along the Murray Ridge and the Owen Fracture zone. The Murray Ridge is thought to be an active rift zone, with extension at the rate of ~0.2 cm/a (DeMets et al., 1990). The Makran subduction zone extends cross-strike 400–600 km from the deformation front in the Gulf of Oman to the Baluchistan volcanic arc. The long trench–arc distance and seismological

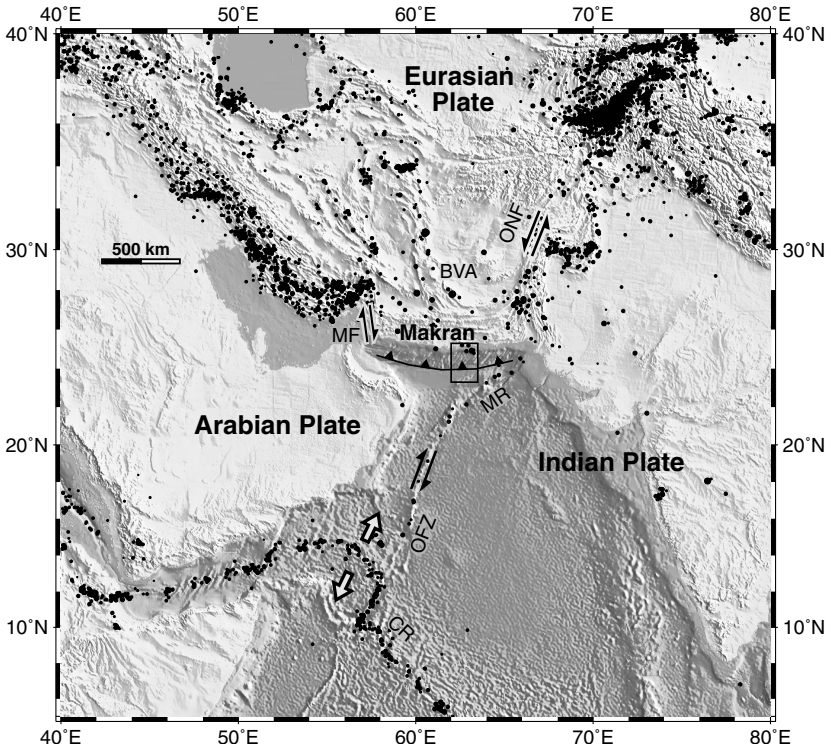

Fig. 1. Location map of the Makran accretionary wedge off Pakistan. Compared to surrounding plate boundaries, the Makran subduction is characterised by sparse earthquake activity (black dots). MF = Minab Fault system, MR = Murray Ridge, BVA = Baluchistan volcanic arc, ONF = Ornach-Nal Fault, OFZ = Owen Fracture Zone, CR = Carlsberg Ridge, rectangle = research area (Fig. 2).

evidence indicate that there is a shallow dipping Benioff zone (Byrne et al., 1992; White and Louden, 1983). This is explained by abundant sediment supply to the trench and substantial sediment transport towards greater depth (subduction/underplating — Jacob and Quittmeyer, 1979). The Arabian plate convergence rate is approximately 4 cm/a in a roughly northerly direction (DeMets et al., 1990), and the wedge grows seaward at an estimated rate of 1 cm/a (White, 1982; Platt et al., 1985).

The oceanic crust in the Gulf of Oman is of almost uniform remnant magnetisation (no reversal patterns have been observed) which suggests formation during a magnetic quiet period. Using models of heat flux measurements, Hutchinson et al. (1981) estimated its age to be 70–100 Ma, which coincides with the Cretaceous M17 "Quiet Zone". This is in agreement with plate reconstruction models from geological observations discussed by Mountain and Prell (1990) and Minshull et al. (1992).

3. Data and methods used

3.1. Acquisition and processing of wide-angle data

In September 1997, during cruise SO123 of the German RV SONNE, five wide-angle seismic lines were shot across and along the Makran accretionary wedge (Fig. 2). The 160-km-long, N–S-trending dip line 8 was chosen to be coincident with the prior MCS-line CAM30. Four E–W-trending strike lines (100–125 km) were shot parallel to the deformation front. Between 7 and 9 OBH were placed along each profile, carefully located between adjacent ridges, parallel to the strike of the ridges. Based on previous studies (White and Klitgord, 1976; Minshull et al., 1992) it was assumed that the accretionary wedge is essentially two-dimensional (2D) with only small variations along strike. Furthermore, these lines were recorded to constrain the expected complex velocity field of dip line 8, which was covered by

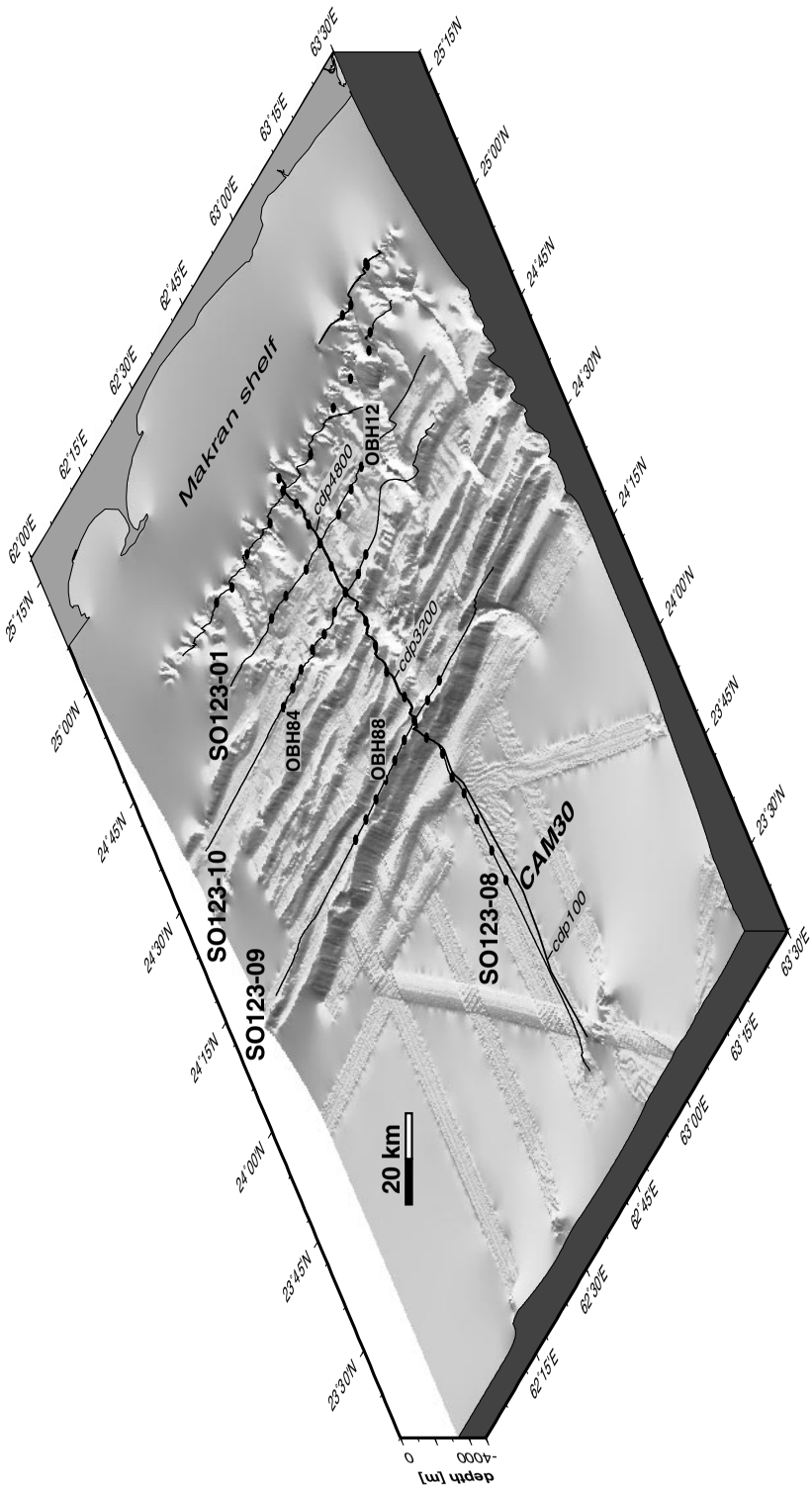

Fig. 2. Bathymetric map of the MAKRAN accretionary wedge with profile- and OBH locations. The labelled lines/OBH are discussed in the text.

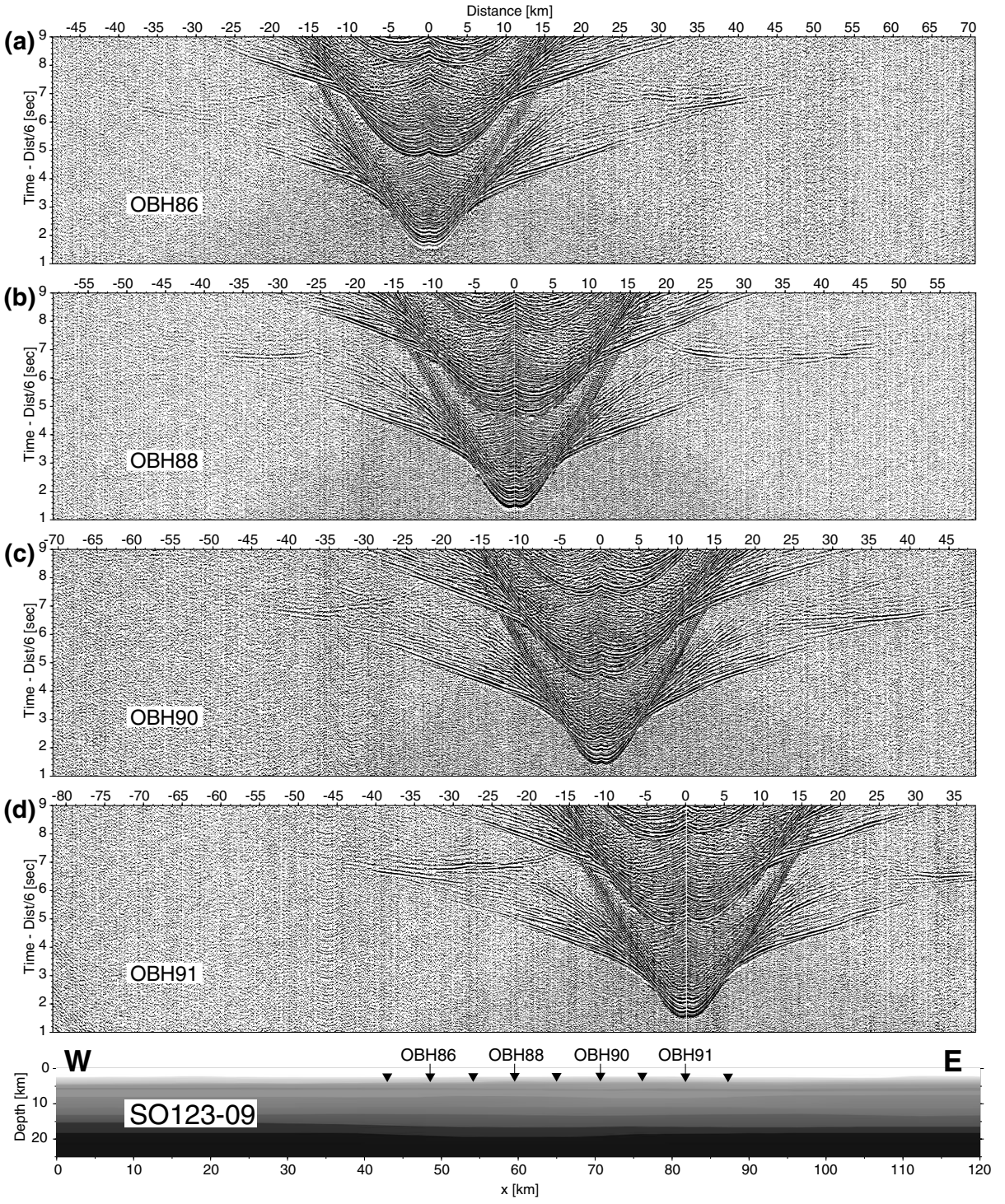

Fig. 3. Four seismic sections from line SO123-09 illustrate the one-dimensional character of most of the E–W-trending lines. Some small differences are limited on deep crustal and mantle phases. With this lateral homogeneity the most important requirement for application of the reflectivity method (Figs. 4 and 6) is fulfilled.

18 instruments. The seismic signal was provided by an airgun array with a volume of 51.2 l. The shot spacing was 120–150 m and recording was done with GEOMAR-OBH (Ocean Bottom Hydrophones) (Flueh and Bialas, 1996) spaced at 4–8 km intervals (locations in Fig. 2). Shooting was extended for up to 50 km from both ends of the instrument arrays.

For an optimal presentation of the wide-angle record sections, time and offset dependent filtering was applied. A time-gated Wiener deconvolution was used to suppress ringing of the signal. For display the sections were weighted linearly with time and offset and reduced at 6 km/s. Interpretation of the wide-angle traveltimes was done using different forward ray tracing approaches (Zelt and Smith, 1992; Luetgert, 1992).

The similarity of the sections shown in Fig. 3 supports the initial 2D assumption: there is little lateral variation in the seismic velocities of the strike lines. Therefore the reflectivity method (Fuchs and Müller, 1971; Müller, 1985) can be applied in addition to kinematic modelling to verify observed relative amplitudes and their variation with offset. Due to the one-dimensional (1D) restriction of the reflectivity method, velocity–depth functions were extracted from the 2D models as input. A precise fit between observed and calculated data is not to be expected. However, because of the smooth lateral variations, useful information on velocity gradients and discontinuities is provided by this method.

3.2. Multi-channel processing and prestack depth migration

Cam30 was recorded by the Bullard Laboratories of the University of Cambridge in 1986 with an airgun array consisting of six guns of a total capacity of 25 l (Minshull and White, 1989).

The two major seismic processing problems of CAM30 were the removal of ringing produced by the collapse of the source bubble, and suppression of multiples. A mixed statistical/deterministic deconvolution approach proved optimal for signal compression and reduction of ringing. Wave-equation multiple attenuation was used in conjunction with radon filtering. Prestack depth migration was performed with a Kirchhoff multi-arrival ray tracing algorithm (most accurate and suitable for complex velocity models). The migration velocities used in Fruehn et al. (1997) were determined from depth-focusing analysis (DFA, cdp 100–3200) and interval velocities derived from stacking velocities (Dix conversion, cdp 3200–4800). The estimated accuracy of DFA-velocities varies between 2 and 10% with depth and degree of deformation, i.e. it should have well-constrained velocities in the abyssal plain and moderate to equivocal results in the wedge below 2 km depth. DFA included the entire sedimentary section above the acoustic basement. A new depth migration presented in Fig. 10 was calculated with the velocities derived from ray tracing of OBH-data from profile SO123-08.

4. Results

All OBH recordings from lines 1, 8, 9 and 10 have been analysed to develop the velocity models shown in this section. They will be discussed from south to north, starting with the E–W lines. Positions of the lines and OBH locations are shown in Fig. 2.

4.1. Line SO123-09

With a length of 120 km, line 9 is placed behind the first accretionary ridge, trending E–W (Fig. 2). The OBH data reveal clear coverage of the accreted sediment down to the basement, crustal and mantle phases occur on most of the stations. Two uncommon features are obvious in the data: articulated near-vertical sediment reflections constrain the bedding and velocity structure of the upper accreted sediment (Fig. 3 and P2, P3 in Fig. 4c). Furthermore, the interpretation of a prominent post-critical reflection (P_{L2} at 6.6 s in Fig. 4c) is unclear. Its differential moveout in the offset range between 30 and 50 km is too large to be interpreted as a mantle reflection.

Crustal phases are present on all lines, and are most pronounced on the southern stations. To the north a complex overburden increasingly attenuates the crustal phases. Although on some stations of line 8 deep crustal phases are stronger, line 9 is an ideal candidate to study the crustal structure off Makran: the thickness of the sediment is still moderate behind the first accretionary ridge and the lateral homogeneity of the subsurface is much higher here than on

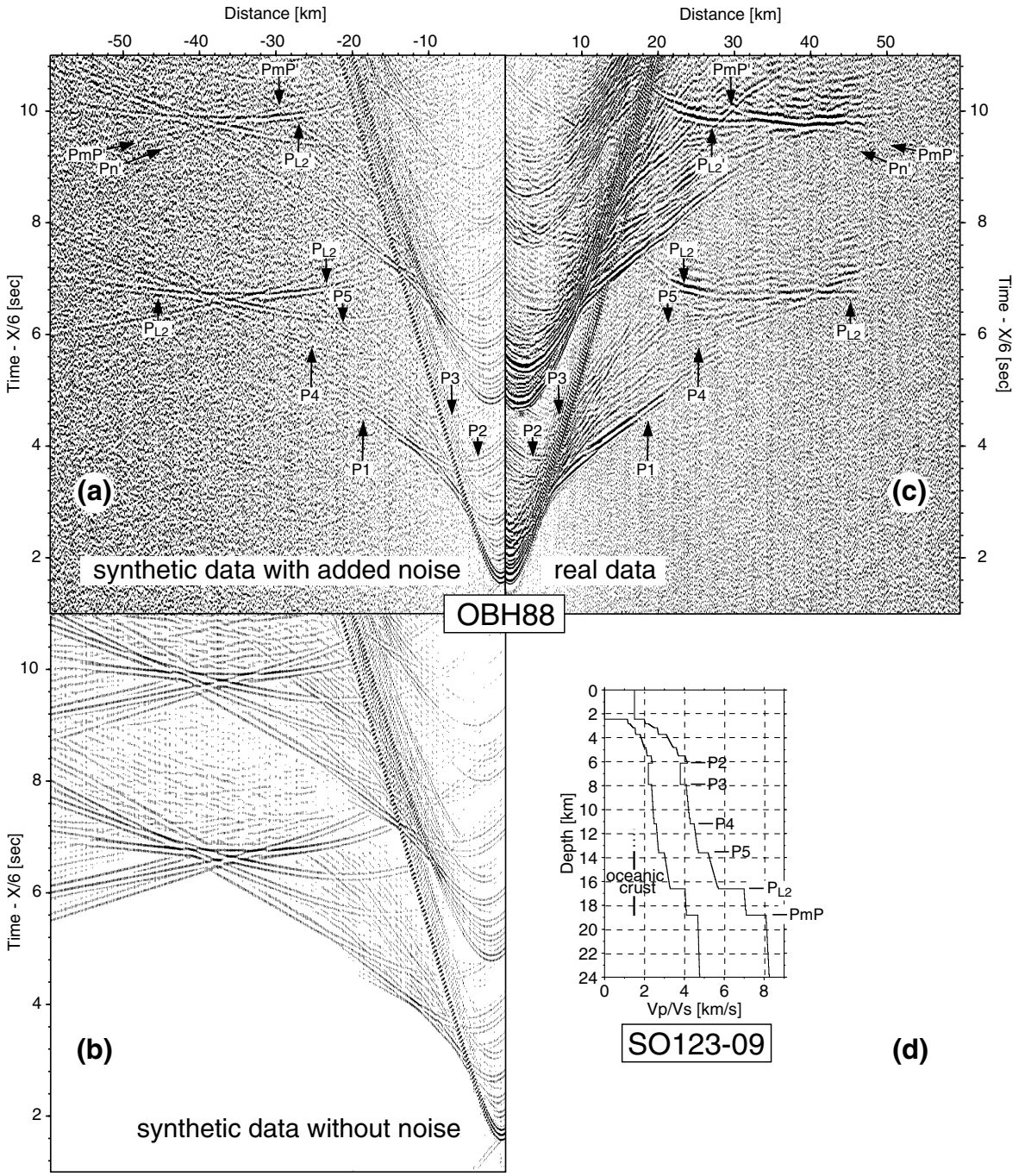

Fig. 4. Observed (c) and synthetic seismogram sections (a) and (b) for OBH88 on line SO123-09. The observed section (c) shows a strong intracrustal reflection (P_{L2}). As its far-offset branch does not exceed apparent velocities of 6 km/s, the first interpretation of a Moho reflection had to be revised. In our interpretation, the reflection is produced by a velocity increase from 5.7 to 7.0 km/s between layer II and layer III. Only in the multiple events can be seen that the weak Moho reflection PmP' crosses P_{L2}.

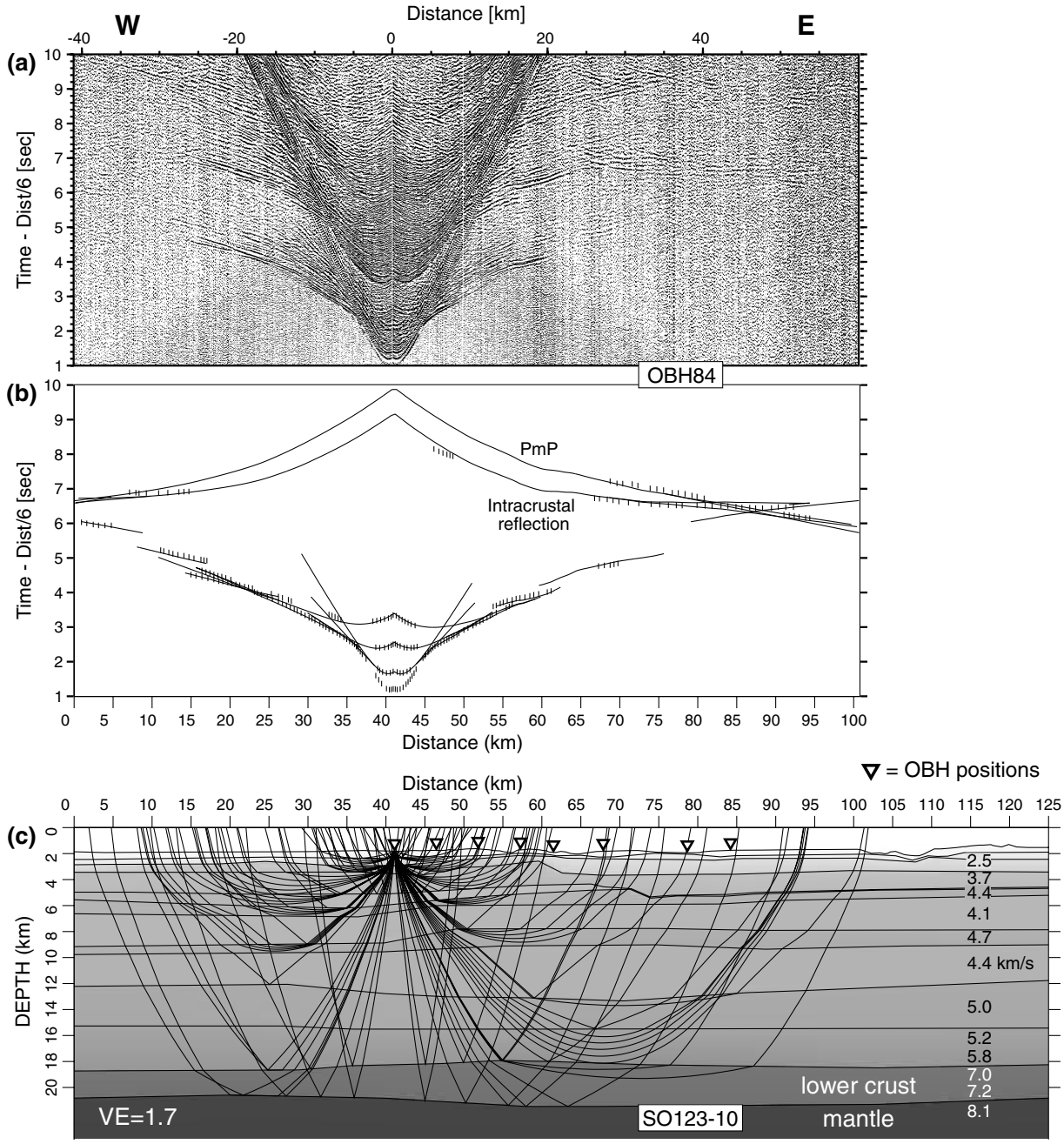

Fig. 5. Data and velocity model of OBH84 (line SO123-10), (a): observed wide-angle section, (b): selected traveltimes (vertical strokes) and computed refraction/reflection traveltimes (solid lines), (c): velocity model of line 10 with raypaths corresponding to computed traveltimes in (b). The observed data show clearly separated PmP and intra-crustal reflections, confirming the structure of the subducting oceanic crust derived for line 9 (Fig. 4).

line 8. Both of these aspects improve identification and correlation of phases between the stations.

Fig. 4 shows a comparison of observed data (c) and synthetic data (a) and (b) for OBH88 on line 9. The underlying velocity–depth-function is illustrated in (d). As lateral changes of the velocities are smooth, this $v(z)$ function is regarded as representative for the entire line. Most of the dominant phases in (c) are successfully modelled by the synthetics. Sediment velocities range from 1.8 km/s at the seafloor to 4.4 km/s near the oceanic basement. A small low-velocity zone (LVZ) is indicated by a refraction dying out at 20 km offset (P1) and the step-back of the first break. Two distinct pre-critical reflections P2 and P3 originate from the upper and lower boundary of the LVZ, which gives a verification of thickness and velocity of the LVZ. From the velocities alone, it is hard to distinguish between sediment and upper oceanic crust. Also the basement reflection cannot be identified definitely. Interpretation of either P4 or P5 as a basement reflection would lead to a crustal thickness of 8.0 or 5.5 km, which are both rather atypical.

The far offset branch of the dominant reflection P_{L2} opposes its interpretation as a Moho reflection because it does not indicate velocities higher than about 6 km/s. Furthermore, P_n (where present as in Fig. 3a) would have to converge with a Moho reflection at about 30 km offset, but seems to cut P_{L2} at a steeper angle. Hence, Fig. 4 illustrates a more likely interpretation of the crustal structure: P_{L2} is interpreted as an intra-crustal reflection between layer II and layer III which has a strong velocity contrast. PmP crosses P_{L2} (at 33 km and 6.7 s in Fig. 4a), although this cannot be seen well in the primary arrivals of the real section. However, the multiple shows this feature clearly: a weak PmP′ crosses P_{L2}' between 30 and 40 km offset in Fig. 4c. Pn is weak on OBH88 in Fig. 4c, but the Moho depth of about 18.8 km is constrained by stronger Pn-phases on the two neighbouring stations to the west. This interpretation results in a velocity gradient of only 0.16 s^{-1} in the upper crust and an extremely high velocity contrast between Layer II and Layer III (5.7–7.0 km/s). The lower crust shows a more usual velocity/velocity-gradient (7.0 km/s/0.05 s^{-1}), but is comparatively thin (2 km). Additional confirmation of this crustal structure is given, for example, by intra-crustal and PmP reflections of OBH84 on line 10 in Fig. 5.

4.2. Line SO123-10

Line 10 also trends parallel to the strike of the accretionary ridges, over a length of 120 km. Located on the landward part of the accretionary wedge, it shows an excellent coverage of the sediment pile. Crustal and mantle phases are attenuated by the thick sediment cover, but still allow for confirmation of the structures derived on the southern stations of lines 9 and 8.

Fig. 5 shows the seismic section of OBH84 (a) and picked traveltimes (vertical lines in b). Sediment layers are represented by reflections and refractions between 5 and 40 km offset. In this range, the first arrivals are discontinuous, indicating the presence of low-velocity zones within the accretionary wedge. Computed traveltimes in Fig. 5b match the picked events including the LVZ-produced gaps in-between. For this figure, only selected reflections have been computed, but since all possible refractions are displayed with their full offset range, the gaps in Fig. 5b are real. Three LVZ were modelled on line 10, the two lower ones labelled with 4.1 and 4.4 km/s in the velocity model in Fig. 5c. The uppermost LVZ at 5 km depth in the western part of the model is only weakly pronounced and pinches out at 70 km. In general there are only a few lateral velocity changes along line 10, except for the area between 60 and 80 km, where velocities decrease from west to east.

The crustal structure, particularly the intra-crustal velocity jump, is similar to line 9. Fig. 5a shows evidence for this anomalous crustal structure: events above 6 s show the existence of a PmP-reflection cutting a gently dipping intra-crustal reflection, as already suggested for OBH88 in Fig. 4. The high amplitudes of this reflection in Fig. 5a again indicate a strong velocity contrast between Layer II and Layer III (5.8–7.0 km/s) while its position relative to PmP confirms a thin Layer III (2–3 km).

4.3. Line SO123-01

Line 1 is the northernmost of the E–W trending lines, with 100 km total length. It is separated from line 10 only by about 15 km. Hence the general features of the two lines are similar: the deeper crustal phases are mostly weak and diffuse, but sediment refractions and reflections are clear. The phase-discontinuities

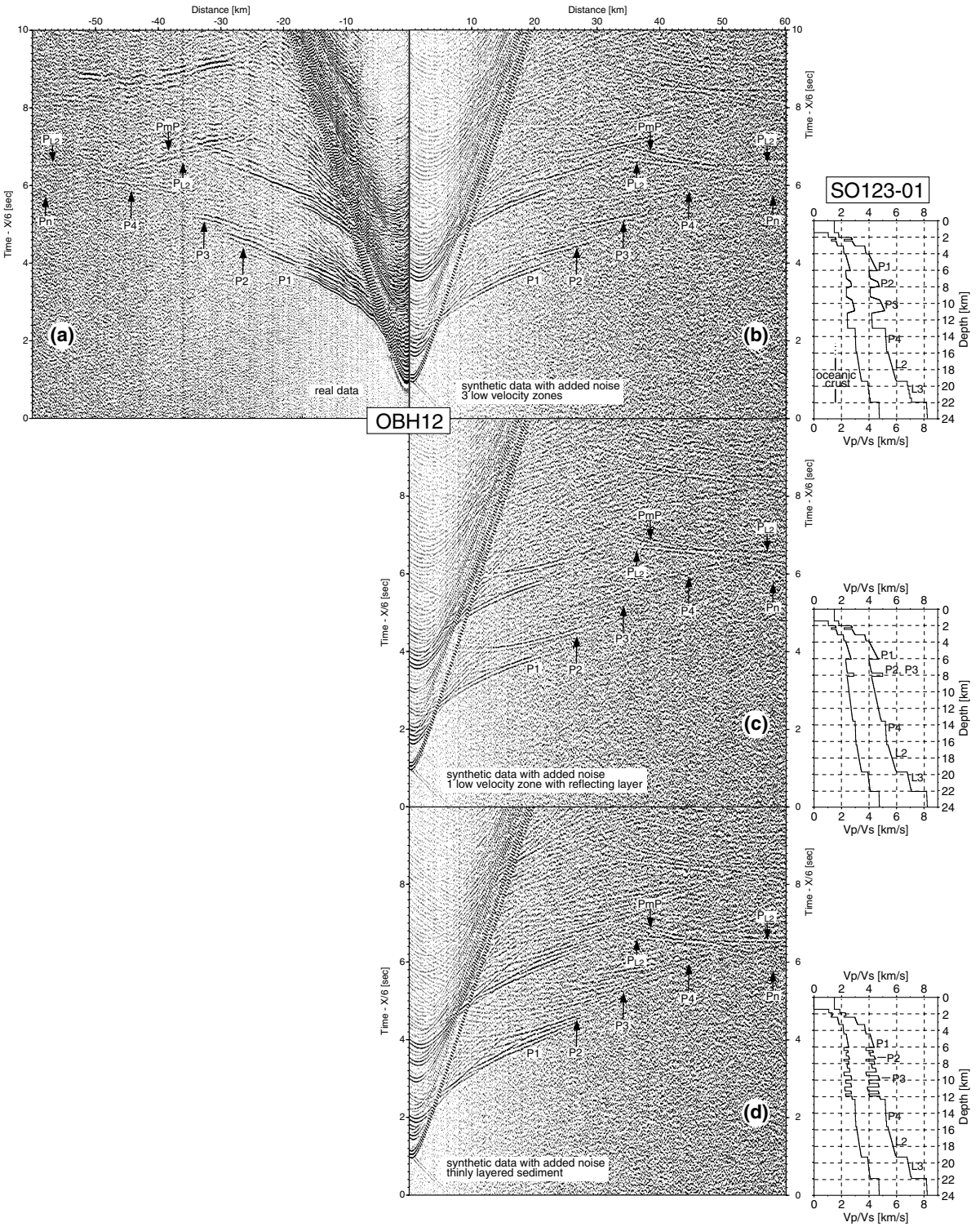
Distance [km]
Time - X/6 [sec]
Pn
PmP
Pl2
P1
P2
P3
P4
(a)
real data
OBH12
(b)
synthetic data with added noise
3 low velocity zones
SO123-01
oceanic crust
L2
L3
Vp/Vs [km/s]
Depth [km]
(c)
synthetic data with added noise
1 low velocity zone with reflecting layer
P2, P3
(d)
synthetic data with added noise
thinly layered sediment

already observed on line 10 occur in a similar shape indicating broad velocity inversions exist also on this line.

Fig. 6 illustrates alternative explanations for the traveltimes of OBH12 on line 1; (a) shows the observed data section and (b)–(d) represent different synthetic reflectivity sections with corresponding velocity models. Phases P_1–P_4 in Fig. 6b correspond to the higher velocity layers in the velocity–depth function. The first continuous event ending in phase P_1 is composed of four sediment refractions from the uppermost layers (revealed by several kinks of the phase in the real data) with velocities between 2.2 and 4.6 km/s. The observed fading of this event and the energy shift to a later phase can only be explained by a LVZ. The structure of the LVZ was estimated using a reasonable seismic velocity and thickness, but since there is no direct velocity information, many different $v(z)$-functions can be found to fit the observed data. Later phases P_2–P_4 can each be explained by only one refractor. To obtain seismic events as in Fig. 6b, velocities must rise continuously from P_1 to P_4, as shown. Strong amplitudes with a limited offset extent and convex curvature observed in P_3 result from a strong velocity gradient within this layer. Previously computed synthetic data-sets with first-order discontinuities enclosing the LVZ showed distinct pre-critical reflections that are not observed in Fig. 6a. It follows that a smooth transition between the different layers is more likely.

An alternative explanation for the shifted phases is illustrated in Fig. 6c. Instead of three LVZ, only one is needed here to fit all observed phases. The low-velocity zone has a larger thickness of about 7.5 km, only interrupted by one reflector, which may be a thicker layer than in this velocity model. In Fig. 6c P_1 is seen as in Fig. 6b, and the LVZ again produces an energy shift affecting the following phases. P_2, reflected at the thin layer within the LVZ, produces several interbed-multiples (P_3 is the first multiple) due to the high reflection coefficient at the base of P_1. P_4 is a refraction from the layer below 14 km depth. A similar case has already been investigated for the crust of the Chugach Mountains (southern Alaska) by Flueh et al. (1989), where peg-leg-multiples on a refraction seismic line were generated by an upper crustal low-velocity zone embedded within higher velocity crust. As P_2 and P_3 originate from the same reflector, they should be strictly parallel (unless the overlying structure does not change significantly in lateral direction). This requirement is more or less fulfilled for the section of OBH12 in Fig. 6, while other sections on this profile contradict the peg-leg model showing higher velocities on the later P_3 phase. Moreover, P_2 and P_3 show distinct refraction characteristics in the real data i.e. convex curvature without significant pre-critical reflection amplitudes. In particular, the primary reflection P_2 in Fig. 6c behaves differently. The amplitudes are also reduced significantly from P_2 to its multiple P_3, whereas in the observed data-set they are more comparable. In the case discussed in Flueh et al. (1989), amplitudes are scaled at x^2, while here they were scaled by x. Multiples are too weak to explain the observed wavefield. A strong velocity contrast at 8 km depth, which is needed to produce high energy multiples, again increases pre-critical reflection amplitudes that are not observed in (a).

Fig. 6d is an attempt to make a more complex, thinly layered accretionary wedge model that one might expect from the observed overthrusting and sediment stacking. This model produces similar en echelon phases as in Fig. 6b and c, but with a highly reflective pattern. It is not wholly consistent with the dominant refraction phases and the low reflection energy such as in Fig. 6a.

4.4. Line SO123-08

Line 8 has a total length of 160 km and covers a wide part of the oceanic basin 65 km off the deformation front. Hence it gives insight to the undisturbed Arabian Plate before passage into the subduction

Fig. 6. OBH12 (line SO123-01) with three alternative interpretations. For the velocity–depth-functions shown on the right, synthetic seismic sections have been computed to explain the parallel phases P1–P4, offset by about 0.2–0.5 s. (a) Observed wide-angle section, (b) separation of layers P1–P4 by low-velocity zones produces an offset in the corresponding refraction events. (c) Multiple reflections within a LVZ produce shifted phases, comparable to (b). (d) A more complex sequence of high- and low-velocity zones explains traveltimes of the observed data, but the multi-reflection pattern differs from the few pronounced events P1–P4 in (a).

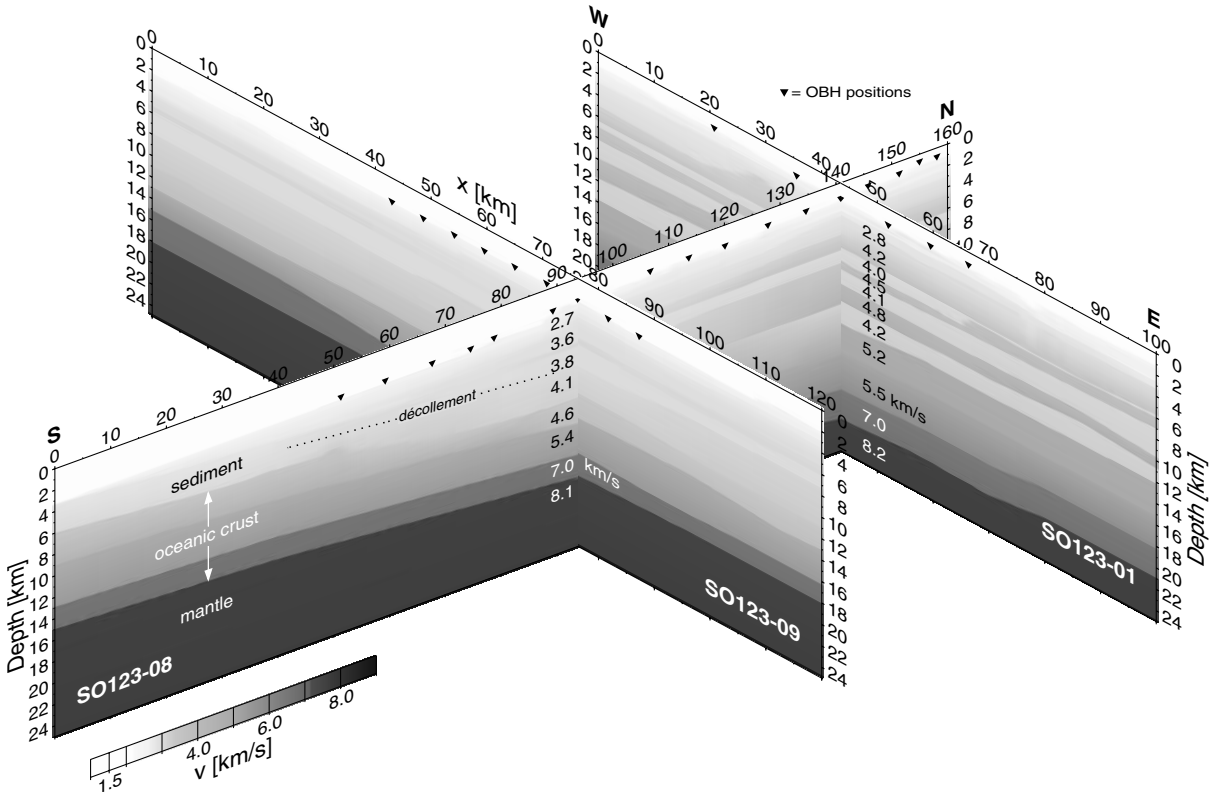

Fig. 7. The wide-angle seismic velocity models display shallow subduction beneath the Makran wedge. As indicated with traveltime- and amplitude analysis, several low-velocity zones are well developed on the E–W trending lines, whereas they can hardly be seen on line 8 due to lateral inhomogeneity of the subsurface. Sediment velocities range from 1.8 km/s at the seafloor to 4.4 km/s near the oceanic basement. North of the deformation front, the oceanic basement is hard to distinguish from the lower sediments, representing an only weak velocity discontinuity. Hence, the crustal thickness is not well determined in some of the investigated regions.

zone. The compilation of velocity models in Fig. 7 shows the S–N trending line relative to lines 9 and 1. Line 8 was shot along CAM30, the only publicly available MCS reflection line in the area. Previous work (Minshull et al., 1992; Fruehn et al., 1997) revealed the wedge structure in detail. It failed, however, to give reliable information from the deeper parts of the section (i.e. the subducted sediments), because of poor constraints on the migration velocities. OBH-data recorded during SO123 along this profile provides these velocities with excellent ray coverage given by the densely spaced instruments.

In the following we present the prestack depth migration of CAM30 obtained from depth-focusing and semblance analysis, discuss briefly the new OBH-velocities, and present the migration of CAM30 with the OBH-velocities.

4.5. Prestack depth migration of CAM30 with near-vertical velocity model

The depth section in Fig. 8 shows an 11 km deep cross-section through the abyssal plain and accretionary wedge. The incoming sediment consists of a ~4 km thick lower sequence of Himalayan turbidites that overlies oceanic crust, and an up to 3 km thick upper sequence of Makran slope-and-shelf sands transported into the Gulf of Oman by deep-cutting canyons (The newly acquired bathymetric data in Fig. 2 show canyons across the wedge). The active deformation front (cdp 2000) is indicated by a gentle fold that is produced by disruption along an upward propagating thrust fault imaged between cdp 2000–2400 in about 6–8 km depth. The horizon from which this thrust emerges is the basal décolle-

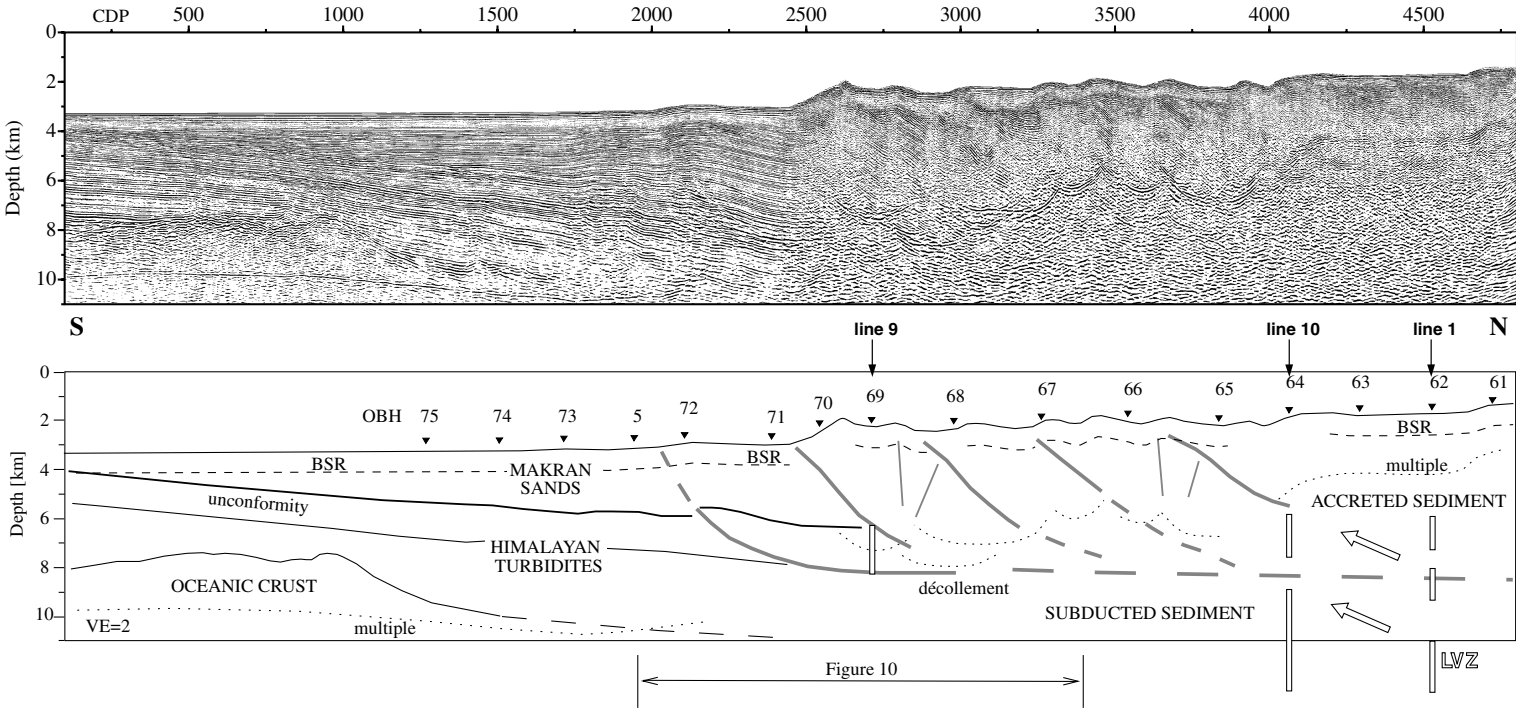

Fig. 8. Prestack depth migration and interpretation of CAM30. The migration was calculated with velocities derived from depth-focusing (cdp 0–3200) and semblance (cdp 3200–4800) analysis. A post-migration radon filter was applied to reduce residual multiples. The interpretation is based on the distinct seismic signature of sedimentary reflectors in the abyssal plain and within the first two thrusts (Fruehn et al., 1997).

ment. It lies within Himalayan turbidites and is a generally continuous and bright reflection. Starting with the first ridge the seismic image deteriorates abruptly, which is probably caused by the steep flanks of the first ridge and the continuing rough ridge-and-trough morphology of the seabed. Technical problems with one of the airguns from this location onwards may also have contributed to a lower signal-to-noise ratio in the wedge compared to the abyssal plain. However, strongly tilted and disrupted reflectors are evident in the upper 4 km of the section. Detailed seismic signature analysis in the most recent and best imaged thrust-fold (cdp 2500–3200; cf. Fruehn et al., 1997), suggests fault-propagation folding of up to 12 km long packages (the distance between deformation front and first ridge), and subsequent secondary faulting that produces an additional ridge at the middle of the package. This mechanism is likely to have shaped the entire wedge, despite substantial variations of fold structure along the line. One possible explanation for these variations is differential erosion experienced by the ridges from meandering canyons. In the depth section of CAM30 (Fig. 8) it is not possible to trace with sufficient confidence any deep reflectors beyond the first ridge. A low signal-to-noise ratio and residual multiples prevents further interpretation. There is also little control on the migration velocities at greater depth, which makes the seismic image less reliable than in the shallow part of the section.

A typical example of data from the abyssal plain segment is shown from OBH74 in Fig. 9a. For ray tracing we have used refractions from the shallow sediments, the reflection from the top of the Himalayan turbidites and from the décollement (where present), reflections from the acoustic basement, and refractions from the oceanic layers (Fig. 9a).

The velocities of the abyssal plain sediments range from upper 1.8–4.0 km/s at 3.5 km beneath seafloor in the south, and increase northward. In the north, at depths greater depth than 10 km beneath seafloor, the oceanic basement is hardly distinguishable from its high velocity sediment cover (Fig. 7). However, in the southern part of the line, the velocity contrast is strong enough to identify the top of the oceanic crust, as confirmed by the acoustic basement reflection seen on CAM30 (Fig. 8). This indicates that here the crust is between 7.5 and 9 km thick. This unusual thickness does not necessarily have to continue beneath the accretionary wedge. The MCS data show that the oceanic basement south of the deformation front is rough and bulged, implying that the crust may be affected by volcanism (Fig. 8, cdp 0–1500). Little Murray Ridge is a feature described by White (1983) that runs parallel to Murray Ridge (Fig. 1) at a distance of about 110 km. Part of its bathymetric expression can be seen in Fig. 2, where ship tracks cross the ridge in the very southern part of the abyssal plain and show bathymetric bulges with an SW–NE trend. Little Murray Ridge crosses CAM30 at its southern tip. Hence, the crustal thickness derived in the south of line 8 is probably not valid for lines 9, 10 and 1, where it may be thinner.

Seismograms from the accretionary wedge segment are distorted due to the ridge-and-trough morphology of the seabed. Deep sediment and crustal arrivals tend to mirror the part of the seabed that the corresponding rays have illuminated (Fig. 9b). Additionally, scattering caused by the irregular seabed and strong lateral velocity variations within the wedge makes these arrivals more difficult to model than in the strike lines. Therefore, we tied-in strike line velocities at the cross points and tried to extrapolate the model parameters to both sides in order to achieve an optimal fit to the data. The model does not show the detailed sequence of LVZ as determined from the strike lines but the important velocity boundaries (décollement, crustal horizons) are generally in good agreement with the structures determined from the strike lines.

4.6. Prestack depth migration of CAM30 with wide-angle velocity model

Migration using the wide-angle velocity model generally reproduced the result obtained using the near-vertical model. There are, however, marked differences in the wedge images (Fig. 10). Because the wide-angle model did not follow the complicated structure of the thrust folds, but rather followed an isoline pattern (see Fig. 7), the fold image is poorer than from the near-vertical velocities. These are closely linked to the structure and were obtained iteratively from depth focusing analysis and prestack depth migration. At depth, however, the wide-angle velocities are more reliable than the near-vertical

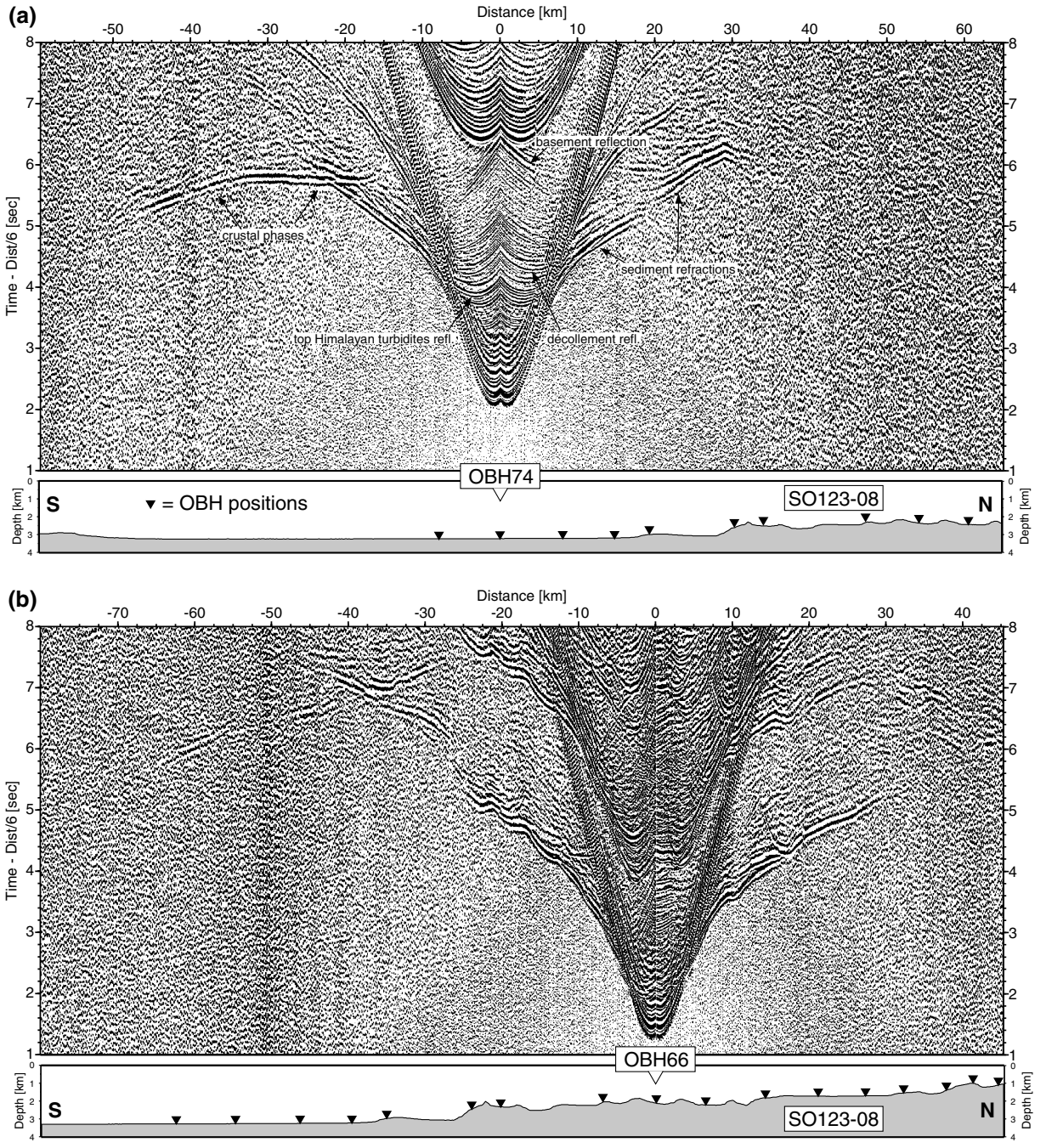

Fig. 9. Data examples from line SO123-08: (a) dominant reflections in the MCS-data interpretation (Fig. 8) can be retrieved in seismic wide-angle recordings from the abyssal plain (near-vertical reflections at offset 0–10 km); (b) refraction- and reflection phases are highly distorted on the northern stations due to a complex morphology of the seabed and strong velocity variations along the line.

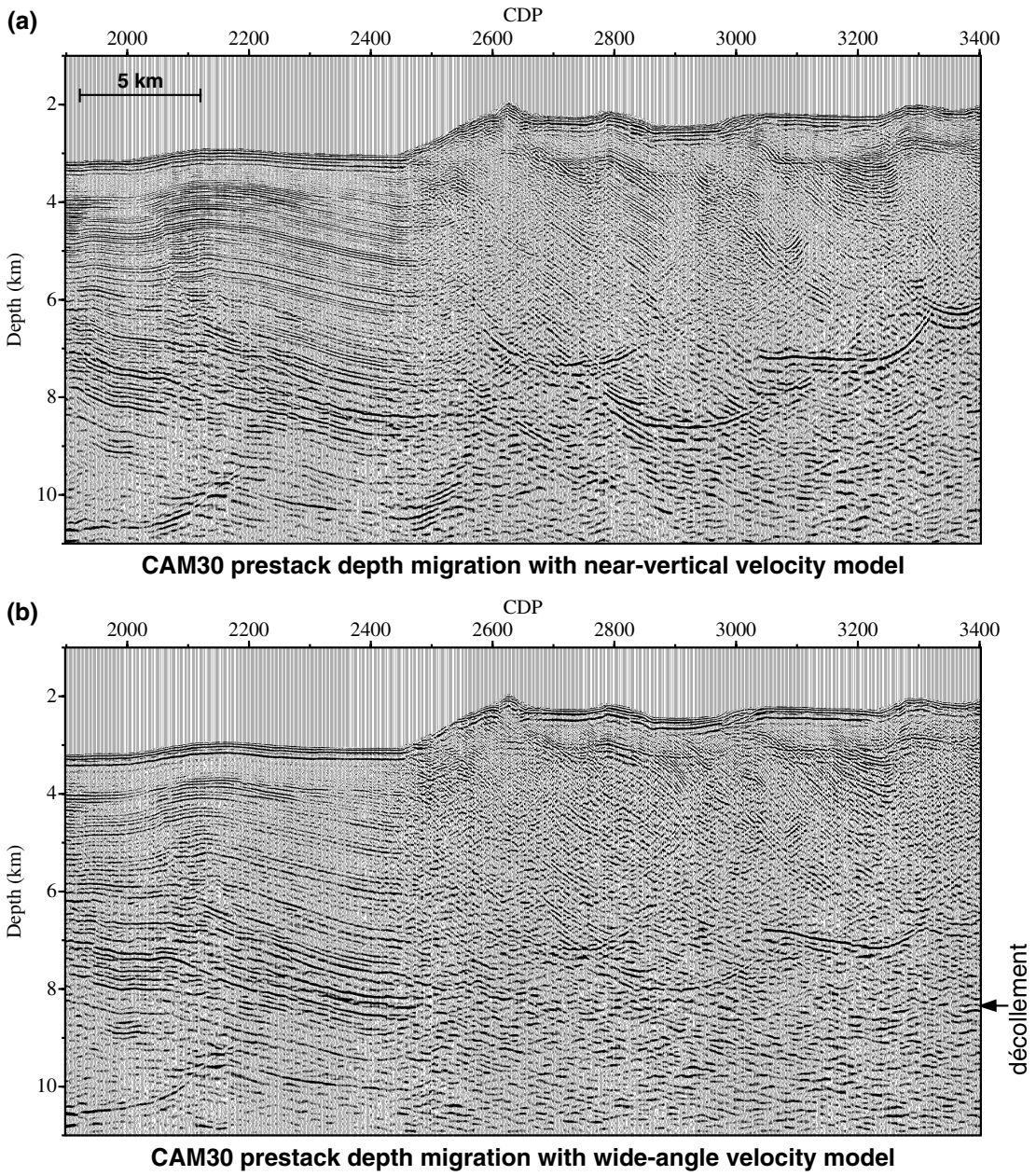

Fig. 10. Comparison of CAM30-migrations with (a) near-vertical and (b) wide-angle velocities. The complex fold structure is imaged better in the near-vertical velocity migration, whereas deep reflectors are better imaged more continuous in the wide-angle velocity migration (décollement cdp 2600–3400 at 8.5 km depth). The vertical exaggeration is 2.0 at the seafloor.

velocities and, hence, so is the seismic image. Despite the abrupt change in seismic signature at the foot of the first ridge (cdp 2500), we can trace the décollement at about 8 km depth well beyond the first ridge (cdp 3000) and, with interruptions, as far as the fourth ridge (cdp 3400). All reflections beneath this horizon are parallel to the subducted plate and there are indications of steeply dipping reflectors above it, once

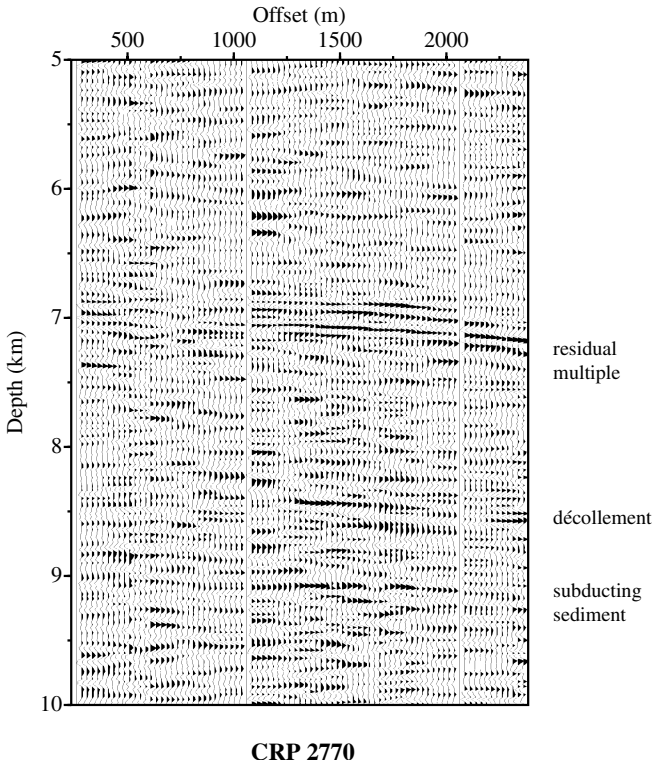

Fig. 11. Example common reflection point gather (crp 2770) that shows flattened deep reflectors below the overmigrated multiple.

again suggesting that this horizon is the basal décollement. To exclude the possibility of having imaged residual multiples, we have analysed common reflection points (crp) from this area. Fig. 11 shows crp 2770, where the flattened décollement reflection is imaged beneath the over-migrated residual seabed multiple.

5. Discussion

The new set of wide-angle seismic profiles provides detailed insight into the Makran accretionary wedge, particularly by the analysis of the E–W trending lines. As lines 9, 10 and 1 run parallel to the accretion structures, each line images the wedge only at a certain level. However, the smooth variation of the structure along these lines provides much more reliable results than does the dip line. Because of strong structural variations, the interpretation of line 8 is ambiguous and does not image all of the small-scale structures of the E–W trending lines. This leads to some velocity model differences at the crossing points in Fig. 7 but, nevertheless, the differences do not represent a contradiction, since the data from line 8 does not rule out the smaller scale structures.

The accretionary wedge shows several low-velocity layers that were modelled on all E–W trending lines. The LVZ are more pronounced towards the north, as indicated by time delays in the refraction events. On the southern line 9 there is just one phase offset (phase P1 in Fig. 4). On the northern line 1 there are four phases distinctly separated by about 0.25–0.5 s (P1–P4 in Fig. 6). Lateral variation is insignificant along these E–W profiles with the phase shifts being observed on most of the stations. This prohibits any regionally limited explanations. The computation of synthetic seismograms illustrates the ambiguities arising from the presence of LVZ. The different velocity models in Fig. 6b–d produce nearly identical results if they are compared for kinematic modelling of only traveltimes. This general problem of velocity

determination within a low-velocity zone can be overcome by identifying pre-critical reflections from the base of the LVZ. On line 9 these phases have been identified successfully. The thicknesses and velocities of low-velocity zones on the other profiles were also estimated. Although the final interpretation of these features is still fairly ambiguous, amplitude analysis (Fig. 6) excludes their interpretation as either peg-leg-multiples or the result of a thinly layered model with many velocity inversions. Only the model with a few, greater than 2 km thick, low-velocity layers shows an acceptable data fit.

There are several possible interpretations for the occurrence of low-velocity zones within the accretionary wedge. Platt et al. (1985) concluded from mass balance considerations and geological arguments that large-scale underplating must have contributed significantly to the growth of the Makran wedge. Underplating occurs in their model only in the landward part. The present study, however, may indicate a seaward continuation of the underplating, if we regard the stack of high and low velocity layers as different underplated sequences. Underplating is also suggested by the recent vertical uplift in the coastal area of Makran (Harms et al., 1984). An alternative interpretation relates the generation of the LVZ closely to thrust faulting within the accretionary wedge. Fig. 8 shows the LVZ-depths of lines 9, 10 and 1 (vertical bars) in relation to the reflection seismic image of CAM30. Except for line 9, the seafloor multiple hides all structural information about the relevant depths, but the uppermost LVZ coincides with the lower tip of some well imaged faults. The direction of thrust faulting in Fig. 8 suggests an inclined correlation of the LVZ as shown by white arrows and dashed lines, rather than the more horizontal correlation seen in Fig. 7. With a northward inclination, the low-velocity layers would not produce continuous events in N–S direction, which could also explain why they can only be seen well on the E–W trending lines. Two effects could be used to explain the velocity inversions; thrust faulting that pushes younger sediment below older sediment, or active dewatering. Assuming that the velocity increases with depth in the undisturbed sediment and the fault slip is sufficient, thrust faulting could produce low-velocity zones beneath the fault planes — which would produce velocity structures like those observed in Fig. 8. However, the extent of the LVZ cannot be explained by this process alone, as the LVZ thickness obviously exceeds the stratigraphic separation, for example see line 9. White and Louden (1983) suggest that deformation and thickening of the accreted sediments continues up to 350 km north of the coastline, which means that faulting, even in the northern part of our sections, is still active. Active dewatering is reported by the occurrence of mud-diapirs throughout the wedge (Kukowski et al., submitted). Consequently, it can be postulated that, at great distances from the deformation front, the generation of velocity inversions may be the result of accretion-connected processes like overpressuring and local dewatering.

A weak LVZ behind the first accretionary ridge at 6–8 km depth is shown clearly on line 9. It cannot be attributed to overpressured underthrusting sediment, since it is located above the décollement, and not below, as would be expected. In contrast, this low-velocity layer must be formed by variations in sediment composition. This is also confirmed by observations on line 8, which suggest a further continuation of this velocity inversion 25 km south of the deformation front. It is not surprising, that — if a LVZ previously exists — the décollement develops at its base, accreting the weak material and underthrusting the solid material.

Even if there are no direct indications for overpressuring, the more than 3 km thickness of subducted sediment may contain enough fluid to explain the sparse earthquake activity at the Makran coast — simply by reducing friction between the two plates.

Our interpretation indicates that this region contains a significant departure from the structure of normal oceanic crust. The upper crustal gradient is too low. In addition, the strong velocity contrast between layer II and layer III is quite unusual, as typical oceanic intra-crustal reflections are low in amplitude compared to basement and Moho reflections. Nevertheless, there are good constraints on the strong differentiation between layer II and layer III. The crustal thickness can only be determined with any certainty south of the deformation front (7.5–9 km), where CAM30 fixes the acoustic basement and the wide angle lines fix the Moho depth. However, it cannot be estimated how much the crust is thickened by volcanic processes. There is no clear identification

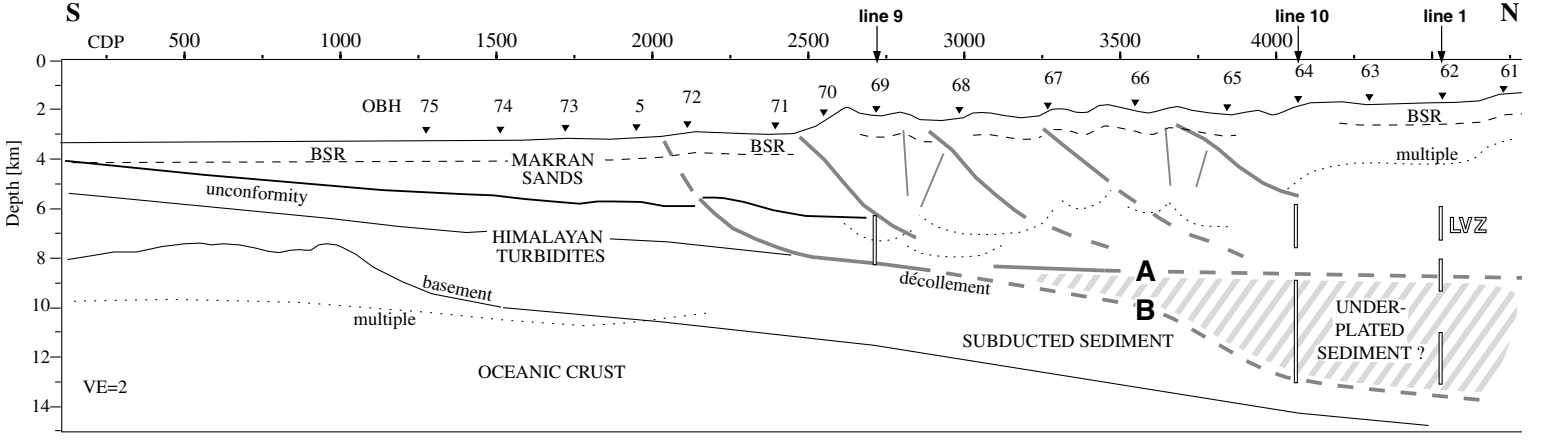

Fig. 12. The structure of the Makran subduction zone. Integration of near-vertical and wide-angle results presented in this paper shows a detailed image of the subduction zone: abyssal plain, accreted thrust folds, the décollement, subducted and underplated sediment, gently dipping oceanic basement. Vertical bars represent the location of low-velocity zones from line 9, 10 and 1 interpretations.

of basement on lines 10 and 1, as the velocity contrast between sediment and crystalline crust is reduced by subduction. Correlation of the strong velocity discontinuity at 13 km depth in Fig. 6b (corresponding phase P4) with the top of basement would imply a total crustal thickness of nearly 9 km. This appears to contradict the clearly identified layer III of only 2 km thickness. Both the depth and thickness of the lower crust are well constrained by the wide-angle data, as illustrated in Figs. 4 and 5. With the known lower crust and the assumption of 7 km thick crust, we estimated the basement depth beyond the first accretionary ridge in Fig. 12. This estimate is in good agreement with the estimate from seismotectonic studies (Byrne et al., 1992). Consequently, reflector "A", discussed in Fig. 12 is too shallow to represent the most recent décollement. On the other hand, the geometry of the wedge (i.e. constant spacing of thrust faults, smooth bathymetry between cdp 2600 and cdp 4000) suggests that the thrust slices have all about the same length, which would imply that "A" is the lower limit of frontal accretion. In our preferred interpretation the décollement steps down from "A" to "B", resulting in the underplating of the hatched section.

6. Conclusions

At Makran, the crust of the Arabian plate is oceanic in character but is quite anomalous in comparison to typical oceanic crust. The crustal thickness is not well-constrained, since the oceanic basement cannot be identified definitively beneath the wedge. It appears that the crust is up to 9 km thick south of the deformation front. The upper crust is characterised by a low velocity gradient (0.16 s^{-1}). Prominent mid-crustal reflections have been modelled by a strong velocity contrast (5.7–7.0 km/s) between oceanic layer II and layer III. The average dip of the Arabian plate in this area is about 3°, which is slightly higher than previously estimated (White and Louden, 1983).

Sedimentary input into the Makran subduction zone is confirmed to be extremely high, reaching 7 km sediment thicknesses at the deformation front. The thickness of Himalayan turbidites is roughly constant (4 km) except where they cover a pronounced basement high. In contrast, the Makran sands thicken from a few hundred metres in the south to about 3 km at the deformation front. The accretionary wedge is found to consist of five uniformly spaced thrust packages, apparently scraped off the Arabian plate along a décollement that lies in the seaward part of the wedge at 8.5 km depth. From the wide-angle study presented in this paper, we conclude that the décollement is stepping down towards the north, thus allowing for substantial underplating. Up to 3 km of the incoming sedimentary section is thrust beneath the first few ridges. The upper part of these sediments is probably entrained by underplating, whereas the lower part is likely to be subducted to greater depths. The lack of a seismic image from this area prevents further quantification. A series of low-velocity zones were found within the wedge. They are probably caused by the thrusting of older, more compacted, sediments over younger sediments. However, the large amount of deeply buried, originally fluid-rich sediment, could also contribute to the formation of low-velocity zones from decompaction and associated fluid release.

Acknowledgements

We thank Captain H. Andresen and his crew on cruise SO-123 for their support and encouragement. We are also grateful to all our colleagues, who participated on the cruise, for their contribution to data acquisition and processing. Richard Hobbs and two anonymous reviewers helped to improve the paper with their constructive comments. The MAMUT project was funded by the German Federal Ministry for Science and Technology (BMBF) with grant 03G00123A and by the EU through the programme Access to Large Scale facilities.

References

Byrne, D.E., Sykes, L.R., Davis, D.M., 1992. Great thrust earthquakes and aseismic slip along the plate boundary of the Makran subduction zone. J. Geophys. Res. 97, 449–478.

Closs, H., Bungenstock, H., Hinz, K., 1969. Ergebnisse seismischer Untersuchungen im nördlichen Arabischen Meer: ein Beitrag zur internationalen Indischen Ozean Expedition. METEOR Forschungsergebnisse, Reihe C, 2, 28 pp.

DeMets, C., Gordon, R.G., Argus, D.F., Stein, S., 1990. Current plate motions. Geophys. J. Int. 101, 425–478.

Flueh, E.R., Mooney, W.D., Fuis, G.S., Ambos, E.L., 1989. Crustal

structure of the Chugach Mountains, Southern Alaska: a study of Peg-Leg Multiples from a low velocity zone. J. Geophys. Res. 94, 16023–16035.

Flueh, E.R., Bialas, J., 1996. A digital, high data capacity ocean bottom recorder for seismic investigations. Int. Underwater Systems Design 18 (3), 18–20.

Flueh, E.R., Kukowski, N., Reichert, C., (Eds.), 1997. FS Sonne Cruise Report SO-123-MAMUT, Maskat-Maskat 07.09.-03.10.1997, GEOMAR Rep. 62, 292 pp.

Fruehn, J., White, R.S., Minshull, T.A., 1997. Internal deformation and compaction of the Makran accretionary wedge. Terra Nova 9, 101–104.

Fuchs, K., Müller, G., 1971. Computations of synthetic seismograms with the reflectivity method and comparison with observations. Geophys. J.R., Astron. Soc. 23 (4), 417–433.

Garzanti, E., Critelli, S., Ingersoll, R.V., 1996. Paleogeographic and paleotectonic evolution of the Himalayan Range as reflected by detrital modes of Tertiary sandstones and modern sands (Indus transect, India and Pakistan). GSA Bull. 108/6, 631–642.

Harms, J.C., Cappel, H.N., Francis, D.C., 1984. The Makran coast of Pakistan: its stratigraphy and hydrocarbon potential. In: Haq, B. U., Milliman, J. D. (Eds.), Marine Geology and Oceanography of Arabian Sea and Coastal Pakistan, pp. 3–27.

von Huene, R., Scholl, W.D., 1993. The return of sialic material to the mantle indicated by terrigeneous material subducted at convergent margins. Tectonophysics 219, 163–175.

Hutchinson, I., Louden, K.E., White, R.S., 1981. Heat flow and age of the Gulf of Oman. Earth Planet. Sci. Lett. 56, 252–262.

Jacob, K.H., Quittmeyer, R.L., 1979. The Makran region of Pakistan and Iran: Trench-arc system with active plate subduction. In: Farah, A., de Jong, K.A. (Eds.), Geodynamics of Pakistan, pp. 305–317.

Kukowski, N., Schillhorn, T., von Rad, U., Huhn, K., Husen, S., Flueh, E.R., MAMUT Working group. The Makran accretionary wedge: Morphotectonic analysis, erosive canoyns, and evidence for shallow gas, submitted for publication.

Luetgert, J.H., 1992. MacRay-interactive two-dimensional seismic raytracing for the Macintosh. US Geological Survey Open File Report, pp. 92–356.

Minshull, T.A., White, R.S., 1989. Sediment compaction and fluid migration in the Makran accretionary prism. J. Geophys. Res. 94, 7387–7402.

Minshull, T.A., White, R.S., Barton, P.J., Collier, J.S., 1992. Deformation at plate boundaries around the Gulf of Oman. Mar. Geol. 104, 265–277.

Mountain, G., Prell, W.I., 1990. multiphase plate tectonic history of the southeast continental margin of Oman. The geology and tectonics of the Oman region, Robertson, A.H.F., Searle, M.P., Ries, A.C. (Eds.), Spec. Publ. Geol. Soc. London 49, 725–743.

Müller, G., 1985. The reflectivity method: a tutorial. J. Geophys. 58, 153–174.

Platt, J.P., Leggett, J.K., Young, J., Raza, H., Alam, S., 1985. Large-scale sediment underplating in the Makran accretionary prism, southwest Pakistan. Geology 13, 507–511.

von Rad, U., Doose, H. (Eds.), 1998. Sonne Cruise SO-130-MAKRAN II-Cruise Report, 3 April–3 May 1998, 152 pp.

Roeser, H.A., 1997. SONNE Cruise SO-122-MAKRAN 1-Cruise Report, 7 August-6 September 1997, 111 pp.

White, R.S., Klitgord, K.D., 1976. Sediment deformation and plate tectonics in the Gulf of Oman. Earth Plan. Sci. Lett. 32, 199–209.

White, R.S., 1982. Deformation of the Makran accretionary sediment prism in the Gulf of Oman (north-west Indian Ocean). In: Leggett, J.K., (Ed.), Trench and Fore-Arc Geology: Sedimentation and Tectonics on Modern and Ancient Active Plate Margins, pp. 357–372.

White, R.S., Louden, K.E., 1983. The Makran Continental Margin: Structure of a Thickly Sedimented Convergent Plate Boundary. Studies in Continental Margin Geology, Watkinsand, J.S., Drake, C.L. (Eds.). Mem. Am. Ass. Petrol. Geol. 34, 499–518.

White, R.S., 1983. The Little Murray Ridge. Seismic Expression of Structural Styles, Bally, A. (Ed.), AAPG Stud. Geol. 15, 1.3.19–1.3.23.

Zelt, C.A., Smith, R.B., 1992. Seismic traveltime inversion for 2-D crustal velocity structure. Geophys. J. Int. 108, 16–34.